# Mid-IR Colloidal Nanocrystals

E. Lhuillier, S. Keuleyan, H. Liu, P. Guyot-Sionnest

**Mid-IR colloidal nanocrystals.**

E. Lhuillier, S. Keuleyan, H. Liu P. Guyot-Sionnest

*James Franck Institute, 929 E. 57th Street, The University of Chicago, Chicago, Illinois 60637, USA*

**Abstract**: Colloidal quantum dots presenting optoelectronic properties into the mid-infrared are reviewed with an emphasis on HgTe. Interband transitions with narrow band gap material and intraband transitions with wide band gap semiconductors can both address the infrared range of wavelengths. Semimetals are particularly promising since, by controlling the particle size, a gap can in principle be opened and tuned through the full infrared spectrum. HgTe has been quite successful recently, and colloidal synthesis has allowed the tuning of the absorption edge from 1 and 5 μm at room temperature. The cut-off wavelength and absorption coefficient of these materials have been discussed. Electrochemistry experiments have demonstrated that both n and p nanoparticles are stable. Films of the HgTe colloidal quantum dots have shown room temperature photoconduction when excited in the mid-IR. With novel processing leading to improved detectivity, these materials are becoming of significant interest as an alternative to the much more expensive epitaxial detector technologies.

**Keywords**: HgTe, quantum-dots, infrared.

**I. Introduction.**

The infrared (IR) spectrum is typically divided into the near-IR (800 nm to 2.5 μm), mid-IR (2.5 μm to 20 μm), and the far-IR (above 20 μm, including THz). Near-IR imaging relies on scattering of an external light source while, above 3μm, the intensity of the black body emission allows thermal imaging. The mid-IR range is also the range of operation of typical infrared spectrometers used for molecular vibrational spectroscopy. In the mid-IR range, there are two transparency windows of the atmosphere, 3-5 μm and 8-12 μm, where ground access to satellite and star light is possible. These ranges are typically called mid-wave IR (MWIR) and long-wave IR (LWIR) respectively, and infrared thermal imaging is targeting these two separate ranges.[1] For single detector applications in scientific spectrometers as well as in infrared motion sensors, pyroelectric materials such as Deuterated Triglycine Sulfate (DTGS) are widely used. However the low sensitivity and low speed of pyroelectric materials does not favor imaging. Thermal imaging is best provided by photovoltaic or photoconducting detectors relying on inorganic semiconductors. In particular, HgCdTe (MCT for mercury cadmium telluride) can be composition tuned to any cut-off wavelength in the mid-IR and therefore optimized for either MWIR or LWIR. MCT has dominated the field for the past 50 years but it has a number of drawbacks including high material cost, cooling requirements, difficulties in obtaining homogeneous chips, and the delicate lithography due to the relative softness of the material. Imaging chips based on MCT provide high quality imaging devices with megapixel cameras, used for military and astronomy applications. However, their more widespread use is limited by high costs, typically in excess of $50,000 for a full imaging system. Alternatives to the MCT are therefore actively sought. The quantum engineering of wider gap materials has led to infrared imaging based on intersubband and intraband transitions of Quantum Well Infrared Photodetectors (QWIP) and Quantum Dot (QDIP) of III-V AlGaAs/GaAs epitaxial materials.[2,3] QWIP provide a viable[4] although still expensive technology. Type II superlattices of InAs/GaSb also allow LWIR photodetection.[5] [6] This epitaxial technology allows higher operating temperatures and is compatible with well-established lithography processes and it is emerging as a very promising alternative.[7]. However, it is still costly and in the development stage. For lower price and lower performance, microfabrication now allows for r microbolometer cameras which operate at room temperature and have good performance in the LWIR but poor performance in the MWIR. At the time of writing this review, the cost of microbolometer imaging systems is still high, on the order of $10,000 for cameras with less than 0.1 megapixels, but they have started to penetrate the consumer market, with a widening range of applications in home insulation

diagnostics, hot-spot trouble shooting in machinery, etc. Novel applications are likely to emerge as the cost of the imaging devices goes down.

Colloidal quantum dots (CQDs) were first studied as rather monodisperse semiconductor nanocrystal precipitates in transparent glassy matrix.[8,9] The liquid phase colloidal synthesis[10] and the ease and precision with which the electronic structure and thereby the optical properties of the material could be tuned with size[11] have since generated much scientific interest.[12,13] In particular, CdSe colloidal quantum dots in the visible spectrum have been widely studied. CQDs can have bright and robust visible luminescence when capped by an epitaxial shell, such as with CdSe/ZnS[14] and other combinations.[15] The fluorescence properties have led to the exploration of biolabelling[16] and light emitting diode[17] applications. Despite great progress, the visible emitting CQDs have not yet displaced technologies based on organic chromophores. The interest in CQDs has extended to the near-infrared with other materials, such as the widely studied PbS/Se CQDs, first in a glassy matrix,[18] and then in liquid solution.[19,20,21,22,23] Much of the current research on the near-IR CQDs is motivated by the hope of CQD thin film solar cells[24,25,26] that might compete with the existing silicon or CdTe technologies and emerging organic photovoltaics. Further into the near-IR, above about 1.5 microns or twice the energy of a CH stretching vibration, the electronic excitation of organic chromophores is very quickly degraded to vibrations. This leads to very low photoluminescence (PL) quantum yields for organics, at best 2 to 3 orders of magnitude lower than typical PbSe CQDs in the same spectral range.[20] In principle, the inorganic cores of the CQDs can allow sustained electronic transitions much further into the mid-IR until close to the optical phonon frequencies in the far-IR. Since CQDs promise low-cost fabrication, with simple processes such as dip-coating, spin-coating, spray-coating, printing etc, they provide an attractive alternative to the expensive procedures required for epitaxially grown materials. In the very high price mid-infrared market, combining these low-cost processing opportunities with the expectation of good optoelectronic properties is a strong motivation for investigating mid-IR CQDs.

A size-tunable mid-infrared response of the CQDs can be obtained by using either intraband or interband transitions. The attractiveness of the former is that any wide band gap semiconductor CQD can, in principle, be used for mid-IR applications including non-toxic materials such as ZnO as well as many other CQDs with well developed colloidal synthesis such as CdTe/Se/S or PbTe/Se/S. However, observing these transitions requires electrical doping. At present, the intraband transitions have been observed transiently after optically

excitation[27] as shown in Fig.1a or by doping by electron transfer[28 29 30 31] as shown in Fig.1b. Although the intraband transitions have been used to learn about the CQDs electronic properties, their further application will require successful impurity-doping[32] of wide band-gap CQDs in the strong confinement regime. However, intraband transitions have not yet been observed by impurity doping. Recently, broad infrared resonances have been reported in heavily doped weakly confined nanoparticles of Al:ZnO[33] as well as non-stochiometric $Cu_2S$.[34] These resonances are plasmon resonances and may be too short lived for some infrared applications but they deserve further study.

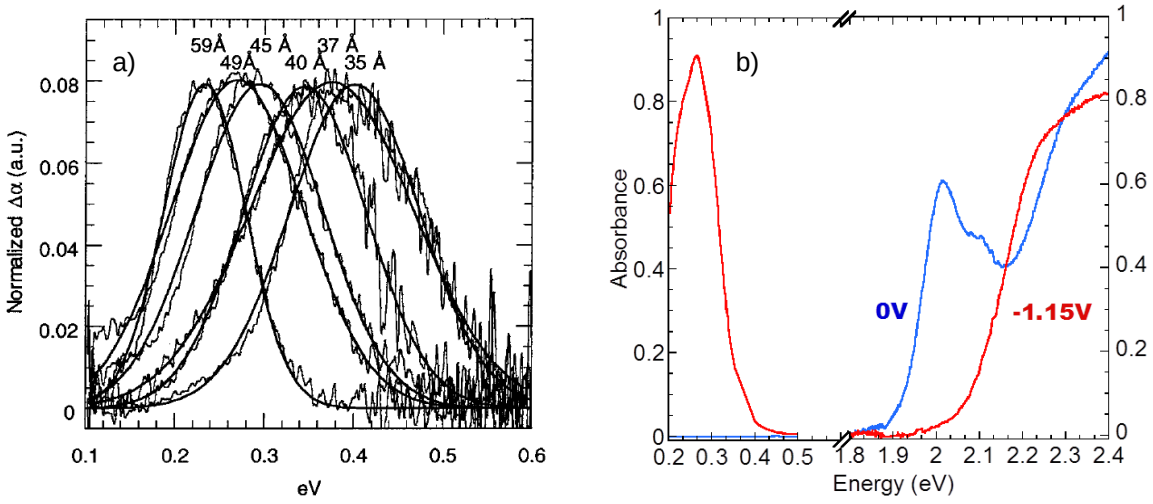


Figure 1 : (a) Transient intraband absorption of photoexcited solutions of CdSe CQDs of the indicated diameters.[35] Reprinted with permission from *J. Phys.Chem.* **2000**, 104, 1494 Copyright. (b) Absorbance spectra of a CdSe CQD film as a negative electrochemical potential leads to electron transfer to the CQDs, with the concurrent bleach of the band edge and rise of the intraband transition.[31] Reprinted with permission from *Appl. Phys. Lett.* **2002**, 80, 4. Copyright [2002], American Institute of Physics..

The use of interband transitions requires narrow gap semiconductors or semimetals in order to reach the MWIR and LWIR. There are several binary narrow gap semiconductors. Bulk PbSe covers only the MWIR, and PbSe CQDs have only been reported with absorption wavelength shorter than 3.6 μm at room temperature.[36] Other binary narrow-band semiconductors including InAs,[37] $Cd_2As_3$,[38] and silver chalcogenides,[39,40] have been investigated but they have not yet led to photoconductivity studies in the mid-IR. Bulk ternary semiconductor alloys can reach further into the LWIR. This includes PbSnSe (Te) and InAsSb. In one study,[41]

nanoparticles of PbSnTe were shown to tune to longer wavelengths than particles of either PbTe or SnTe.

In contrast to semiconductors, semimetals have no intrinsic limitation towards long wavelength. For example, when graphene will be synthesized as strips or dots with well defined sizes, it could provide an interesting IR material.[42] Among the binary materials, the mercury chalcogenides have a special place since they are semimetals with a particularly simple band structure. In particular, bulk HgTe has been extensively studied[43,44,45,46,47,48]

**HgTe material parameters**

Table 1 : parameters related to the HgTe material

| **Parameter** | **Value** | **Unit** | **Reference** |
|---|---|---|---|
| Molar mass | 328.2 | $g.mol^{-1}$ | |
| Lattice parameter | 0.646 | Nm | [49] |
| Lattice structure | Zinc Blende | | |
| $E_G^{bulk}(T)$ *Bulk band gap* | $-303+\frac{0.63}{11+T}$ | meV | [50] |
| $E_P$ *Kane Energy* | 18 | eV | 50 |
| $\Delta_{SO}$ *spin orbit coupling* | 1 | eV | 50 |
| $\varepsilon_0$ *Static dielectric constant* | 20 | | [51] |
| $\varepsilon_\infty$ *Dielectric constant at optical frequency* | 14 | | [49] |
| $\hbar\omega_{LO}$ *LO phonon energy* | 17±3 | meV | 52 |
| ρ*the mass density* | $8.1\times10^3$ | $kgm^{-3}$ | 49 |

Several of its properties are listed in Table 1. Unlike CdTe, the Hg s-like orbital is lower in energy than the Te p-like orbital. This results in an inverted band structure with a zero-gap

where the conduction band is the light hole and the valence band is the heavy hole. The band structure is shown in Fig. 2. This inverted structure crosses back to the normal ordering at the free surface or at the interface with CdTe which leads to a Dirac cone for the dispersion at the surface/interface and this opened the use of HgTe as a topological insulator.[53] The discovery of the quantum spin Hall effect[54] was done with a quantum well structures of HgTe/HgCdTe with a 6.3nm or thicker HgTe layer. In addition to transport studies conducted on pure HgTe, the HgCdTe alloy has long been investigated for infrared detection purposes. As mentioned earlier, this is the dominant mid-IR material for photodetection where, with a precise cadmium concentration, the optical gap tunes from zero to the gap of pure CdTe.

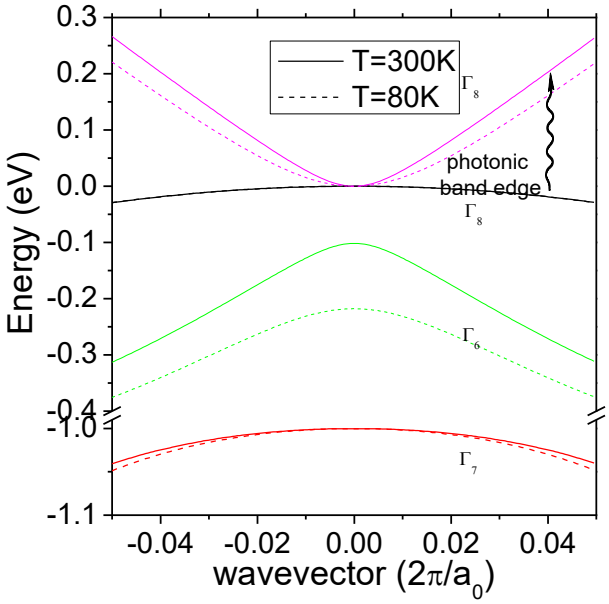


Figure 2: band structure at 300K of HgTe near the center of the Brillouin zone and in the 8x8 k.p approximation. The dashed lines are for the 80K bulk band gap. Parameters are from ref.50.

**II. Synthesis of HgTe CQDs.**

The indication that HgTe was promising as CQDs was first provided by Rogach et al.[55] In an aqueous colloidal synthesis, HgTe nanoparticles of 3 to 6 nm diameter were produced with luminescence near 1.3 mm, covering the first telecom band. Weller and coworkers continued to investigate the synthesis of HgTe CQDs in the early 2000's[56], including work on HgTe/CdS core/shell structures[57]. Their method was based on the reaction of $Hg(ClO_4)_2$ dissolved in a basic aqueous solution with $H_2Te$. This allowed the bandgap to be tuned across the near-IR as far as 1.8 μm. Kovalenko et al modified this method in 2006. By adding an

Ostwald ripening step at elevated temperature, followed by transfer to a nonpolar phase and size-selective precipitation, particles of ~10 nm with PL close to 3μm were obtained.[58] In addition to size, the bandgap can be controlled through composition, as is done in bulk MCT. Alloying was reported starting directly with a mixture of mercury and cadmium precursors with however very modest tuning into the near-IR up to 850 nm [59] $Hg_xCd_{1-x}Te$ alloy particles have also been prepared via $Hg^{2+}$ cation exchange on CdTe particles[60,61] as well as one-pot reactions[62,63] showing high PL quantum yields, but these studies were also limited to the near-IR. In parallel with the development of the aqueous synthesis, Green et al[64] reported a synthesis of HgTe directly in organic solvent. The synthesis was based on the reaction of mercury bromide with tellurium complexed with trioctylphosphine (TOP), noted as TOP:Te, in octadecylamine as a coordinating solvent. The resulting nanocrystal colloidal material was HgTe and crystalline but polydispersed with a broad absorption spectrum that did not allow assigning a band edge, and there was no detectable PL. In 2006, Piepenbrock *et al*[65] developed a related synthesis using mercury acetate in chilled alcohol in presence of hexadecylamine and TOP:Te. Using this approach, a clear absorption edge was observed in the near-IR and PL up to 1.6 μm was reported. With pure HgTe, the k.p band structure in Fig. 2 shows that 3 to 5 μm band-gaps would be realized with particles of sizes between 8 and 12nm. Expanding on the method introduced by Piepenbrock et al, the reaction between mercury(II) acetate and TOP:Te in butanol in the presence of pyridine led to larger HgTe particles allowing, for the first time, to cover the MWIR.[66] Briefly, 0.1 mmol (13 mg) Te powder was dissolved in 2 mL butanol using 0.1 mL TOP at 90°C. Meanwhile, 0.1 mmol (32 mg) mercury(II) acetate was dissolved in 2mL of butanol with 2mL pyridine. The mercury acetate solution was then rapidly injected into the flask containing the TOP:Te, with the solution immediately turning black, indicating the formation of HgTe. Absorption spectra of HgTe CQDs prepared by this method are shown in Fig. 3c. The absorption edge is not very sharp, showing an excitonic shoulder rather than a peak. This is due to rather broad size distribution. Furthermore, dynamic light scattering and Transmission Electron Microscopy (TEM) indicated partial aggregation of the dots in the solution. Subsequently, a preparation more similar to that of Green et al. yielded more monodisperse nanocrystals with an exciton peak at the band edge.[67] In this preparation, $HgCl_2$ is dissolved in oleylamine and reacted with TOP:Te, giving controlled growth and well defined excitonic absorption peaks from 1.4 to 5 μm. Technical grade (70%) oleylamine presents batch to batch variations which lead to undesireable variability in the synthesis. Octadecylamine (ODA) can be used in place of

oleylamine to give more consistent results, with the inconvenience that it solidifies below 52°C.

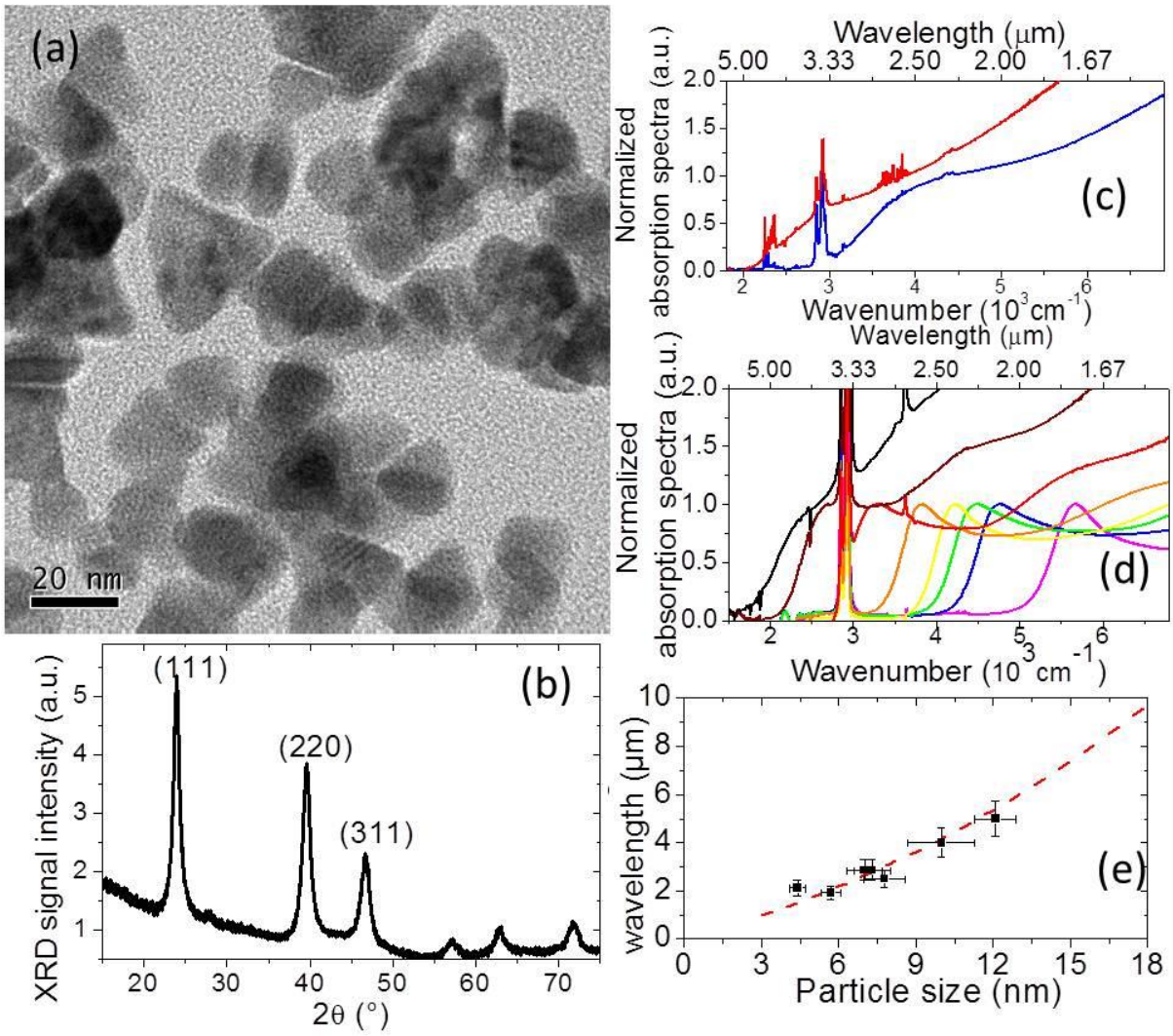


Figure 3: (a) TEM image of HgTe CQDs.[67] (b) X ray diffraction of HgTe CQDs. (c) Absorption spectra of solutions of HgTe CQDs of two sizes.[66] (d) Absorption spectra of more monodispersed HgTe CQDs.[67] (e) Exciton wavelength of HgTe CQD as a function of the CQD size. The dashed line results from a k.p simulation.[68]

In a typical synthesis, 0.1 mmol $HgCl_2$ and 3.5 g ODA are heated under vacuum to 120°C for 1 hour to degas. The solution is then cooled under Ar to the growth temperature determined by the desired size. 0.1 mL 1M Te in TOP is then quickly injected and the solution darkens at a rate dependent on the temperature, typically appearing black within 30 s or less. TEM images, X-ray Diffraction, and absorption spectra of the CQDs are shown in Fig. 3. The HgTe materials are in the stable bulk zinc-blend phase. After the reaction, the HgTe particles can be

capped with dodecanethiol, which stops the growth and allows stable dispersion in tetrachloroethylene (TCE) for storage. Since the excess ligand and solvent are opaque in the infrared, the dots need to be extracted for optical characterization. The dodecanethiol capped HgTe dots are easily precipitated using methanol. The precipitate can then be rinsed, dried and redispersed in neat TCE, yielding a solution that is stable in air for weeks to months, and which can be used for absorption and PL measurements. [68]

Films of the HgTe CQDs can be obtained by directly drying the TCE solution. Better uniformity can be achieved by precipitating and redispersing in a 9:1 (vol.) hexane:octane mixture. Thicker films can be prepared by depositing multiple layers, fixing each before depositing the next using a dilute solution of shorter ligands such as ethanedithiol. Improved adhesion to the substrate can be achieved by treating the substrates with mercaptopropyltrimethoxysilane for glass substrates or a dithiol for metal electrodes.

*Safety:* The acutely lethal organomercury compounds are avoided, but mercury(II) salts are toxic and appropriate precautions must be taken to avoid exposure or release into the environment. HgTe is considered a toxic compound as well as a hazardous product for the environment. The handling of the material requires the appropriate safety equipment including eye protection, gloves and labcoat. Associated risk codes are R26, R27 R28, R33, R50 and R53, while the safety phrases are S13, S28, S45, S60 and S61.

**III. Optical properties of HgTe CQDs.**

The size control afforded by the methods described above allows the room temperature optical bandgap of HgTe CQDs to be tuned between 1.2 and 5 μm. A two-band k.p model provides a fair prediction of the bandgap as a function of particle size as shown in Fig. 3e. [68]

Within the two-band k.p model, an analytical expression of the particle bandgap is given by

$$E_{BE}^{QD} = \frac{E_G}{2} + \sqrt{\frac{E_G^2}{4} + \frac{2}{3} E_P \frac{\hbar^2 k^2}{2m_0}} \qquad (1)$$

where $E_G$ is the bulk band gap of HgTe, $E_P$ is HgTe Kane parameter and $k = \pi / R_{QD}$ is the wavevector associated with the ground state transition assuming a complete confinement of the carrier within the CQD. The parameters used are given in Table 1. Using Eq.1 and a best

fit to the data, the wavelength of the first interband transition (in μm) as a function of nanoparticle radius ( $R_{QD}$ in nm) is given by the empirical expression

$$\lambda_{BE}^{QD} = \frac{30.5}{\sqrt{1+\left(43/R_{QD}\right)^2}-1} \qquad (2)$$

In addition to varying with particle size, the optical-gap also changes strongly with temperature. Like bulk HgTe, HgTe CQDs show a redshift of the band edge transition upon cooling. As shown in Fig. 4a, the absorption band-edge wavelength of the largest size samples shifts from 5μm at room temperature to 7μm below 80K. $\frac{dE_{BE}^{QD}}{dT}$ is weaker for the smaller particles, as shown in Fig. 4b. This is a similar behavior to that seen for PbS CQDs. [69] In contrast, CdSe[70] shows a size-independent negative $\frac{dE_{BE}^{QD}}{dT}$. Most semiconductors exhibit a negative *dE/dT* which is attributed to the thermal expansion and to the second order perturbation of the intraband electron-LO phonon coupling. However, several narrow gap semiconductors, including the II-VI Hg-chalcogenides and the IV-VI Pb-chalcogenides have a positive *dE/dT*. An interpretation is that, in narrow band gap materials, the interband electron-LO phonon coupling second-order contribution which is positive, can be larger than the intraband part. As the size is reduced and the gap increases, the positive interband contribution decreases, leading to a smaller temperature tuning of the band edge. Such effect is seen in CQDs of PbS,[69] PbSe[71] and HgTe.[68]

A key parameter for the use of the HgTe CQD in optoelectronic devices is the material absorption strength. In contrast to self-assembled epitaxial quantum dots, which have been investigated in QDIP, the CQDs allow close-packing. In addition, there is a transfer of the oscillator strength to the QD band edge. Therefore the optical absorption edge of HgTe CQDs films could be even stronger than the bulk MCT. This absorption can be quantified in solution as an absorption cross-section per particle, or for a film as an absorption coefficient. Using acid-digestion and Hg titration with dithizone, the molar concentration of Hg was determined for CQDs of various sizes and compared to the optical density.[68] To get an absorption cross-section per particle, the particle size was estimated from the XRD peak-width. Far above the band edge, at 415 nm, the cross section per mercury atom is almost constant and equal to $2.6\times10^{-17}$cm$^2$ and this can then be used for analytical purposes. The lowest-energy transition cross-section per particle was found to be ~$1.5\times10^{-15}$cm$^2$ with a weak

size dependence. The integrated band edge cross-section, which better accounts for the sample to sample polydispersivity variation, was ~$10^{12}$cm, as shown in Fig. 4c and it has been satisfactorily compared to the k.p model. For films, the absorption coefficient has been measured as well. Experimental and k.p modeling of this parameter are displayed on Fig. 4d. The absorption coefficients of the films of HgTe CQDs are indeed as high or higher as those for bulk HgTe[72] or bulk HgCdTe alloys[73,74,75] with a similar cut-off wavelengths.

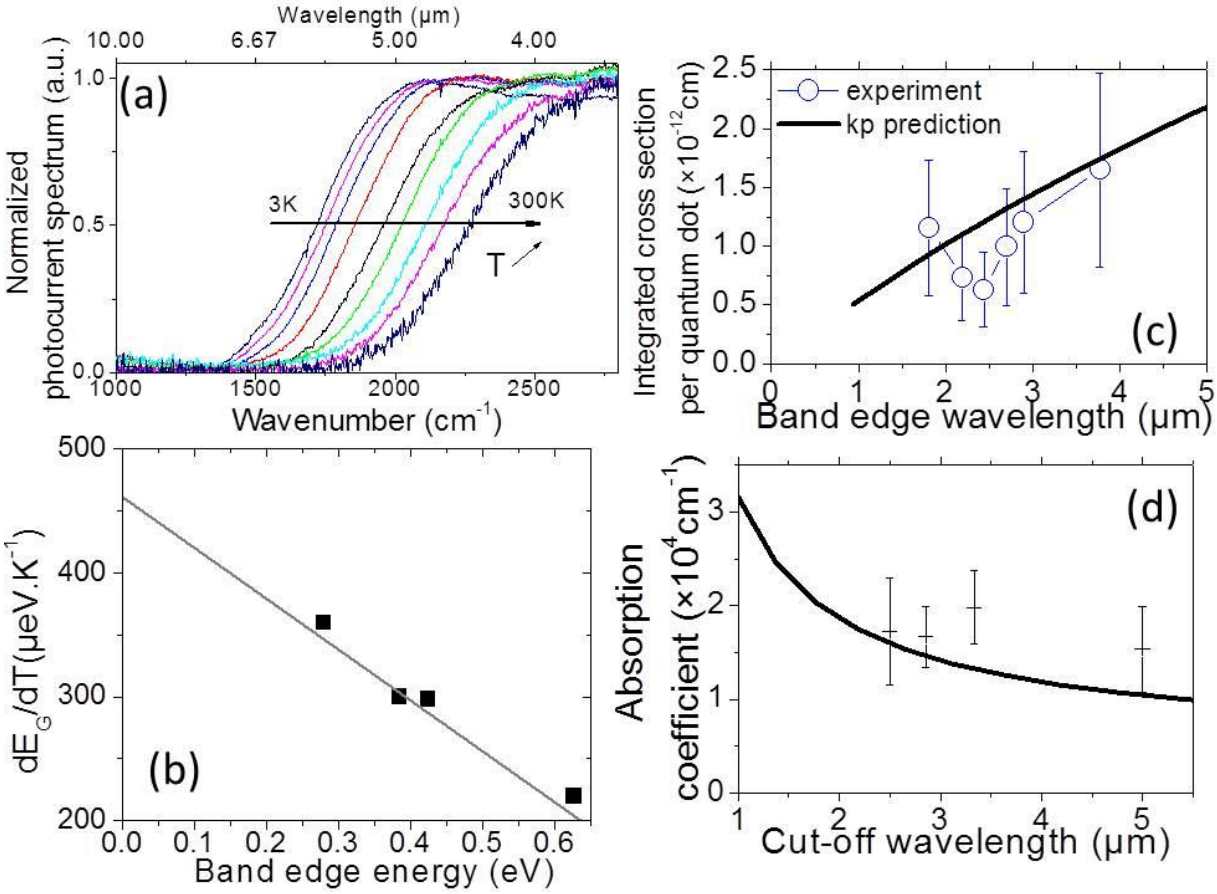


Figure 4: (a) Photocurrent spectra of a film of ethanedithiol cross-linked HgTe CQDs at different temperatures. (b) Thermal dependence of the band edge energy as a function of the room temperature band edge energy for HgTe CQD of different size. (c) Integrated cross section per quantum dot as a function of the exciton wavelength. The solid line results from a k.p simulation. (d) Absorption coefficient of HgTe CQD film as a function of the exciton wavelength. The solid line shows results from a k.p simulation.[68]

In principle, the inorganic CQDs should allow efficient mid-infrared fluorescence. While PbSe CQDs are quite fluorescent in the near-IR with quantum yield , the PL intensity drops dramatically in the mid-IR.[36 76 77] HgTe CQDs simply capped with thiols have been shown early on to have efficient band edge luminescence in the near-IR,[55] indicating that deep

trapping does not occur readily at the surface. As expected, larger HgTe CQDs exhibit PL in the mid-IR, albeit with lower yields.[67]

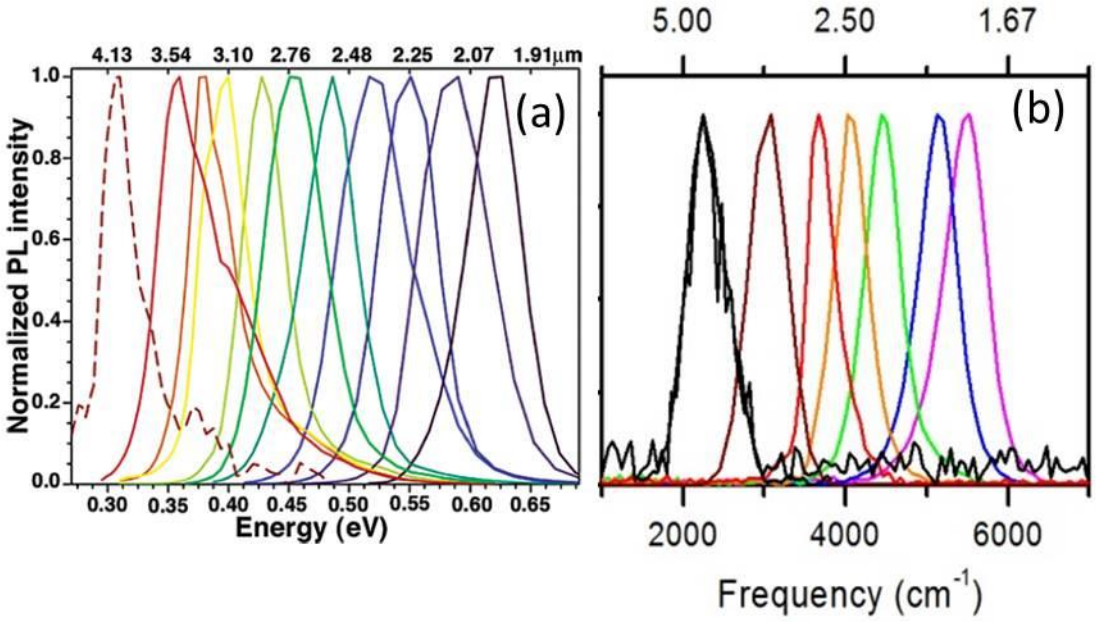


Figure 5: Room temperature PL spectra of (a) PbSe CQD of different sizes (dashed curve measured at 77K), adapted with permission from *J. Am. Chem. Soc.* **2004**, *126*, 11752, Copyright (2004) American Chemical Society(b) HgTe particles prepared in ref.[67] adapted with permission from *J. Am. Chem. Soc.* **2011**, *133*, 16422-16424

Fig. 5b shows PL spectra of HgTe CQDs. It has been noted that organic ligands not merely reduce transmission of the materials in the mid-IR, but more importantly provide an extremely efficient near-field energy transfer from the inorganic core electronic excitation to surface molecular vibrations.[78] Such an effect has been reported to affect the PL quantum yield of near- IR CQDs of InAs[79] and PbSe,[76 77] as well as to cause fast intraband relaxation.[78 80] Therefore inorganic matrices and core/shell structures will be beneficial. Besides the wide tunability of the CQDs, one advantage of HgTe compared to the lead chalcogenides is the greater simplicity of the band structure, including the zero gap and the non-degeneracy of the band edge. This results in a smaller density of states at the absorption edge, which should facilitate population inversion and reduce Auger recombination rates. On the other hand, surface states arising from the inverted band structure that is specific to HgTe might enter the gap at large enough sizes, creating the possibility of additional recombination channels. The HgTe mid-IR PL properties have not yet been thoroughly characterized, but they might be of

interest in LEDs or lasers, either by direct electrical pumping or by using near-IR optical excitation. The characterization of the PL of the material will require the determination of the PL lifetime, quantum yield, carrier lifetimes, Auger processes, nonradiative recombination processes, and stimulated emission properties. The HgTe CQDs therefore warrant much further investigation of the PL properties.

**IV. Electronic properties of HgTe CQD**

Transport in HgTe CQDs has been first characterized using thin solid film field-effect transistors (FET).[81,82,83] By annealing films of thioglycerol capped nanocrystals, high mobility FET, with $\mu \approx 1$ $cm^2V^{-1}s^{-1}$ and good on/off ratio $\approx 10^3$, were obtained. However, the material showed only p-type transport and no optical data was reported. With unannealed samples made using an inkjet printer, Heiss and coworkers demonstrated photoconduction up to 3 μmfor their largest particles but there was no study of the conduction mechanism or of the carrier mobility.[84] In general, knowing the absolute energy position of the valence and conduction bands will give some insight into the relative stability of electrons and holes in the quantum dots. Electrochemistry is therefore an advantageous characterization tool for CQDs. Electrochemistry of HgTe CQDs has allowed determining that both n and p-type charging was possible in anhydrous conditions with moderate reduction or oxidation potentials, as shown in Fig. 6a and 6b. In addition, the bleach of the optical spectrum and the rise of intraband absorptions were monitored, confirming that both n and p-charging corresponded to carrier injection in the quantum dot states instead of surface states. Based on the interband bleach and intraband absorption as a function of charge injection, an energy level diagram of the CQD states for two different sizes was reconstructed as shown in Fig. 6c. It was noted that, although the band edge energy was well accounted for by the k.p model of a spherical box, the higher lying transitions of the bleach spectra could not be matched well to the expected states of the spherical quantum dot, an effect which was attributed to the non-spherical shape of the nanocrystals. A tight-binding calculation has been developed for HgTe nanocrystals of different shapes.[85] Although fair agreement was found with the band edge absorption energy, further comparison between theory and experiment will require the synthesis of HgTe nanocrystals with better defined shape.

In contrast to the previous FET results, electrochemistry showed than both n and p-type transport is effective, with similar magnitude of n and p-mobility. It was also noted that the photocurrent was 100x larger for p-type, while photocurrent decays following transient illumination were 100x slower for p-type than for n-type, as shown in Fig. 6d. This was

assigned to an electron trap cross-section 100x smaller than that for holes but the recombination mechanism has not been investigated.

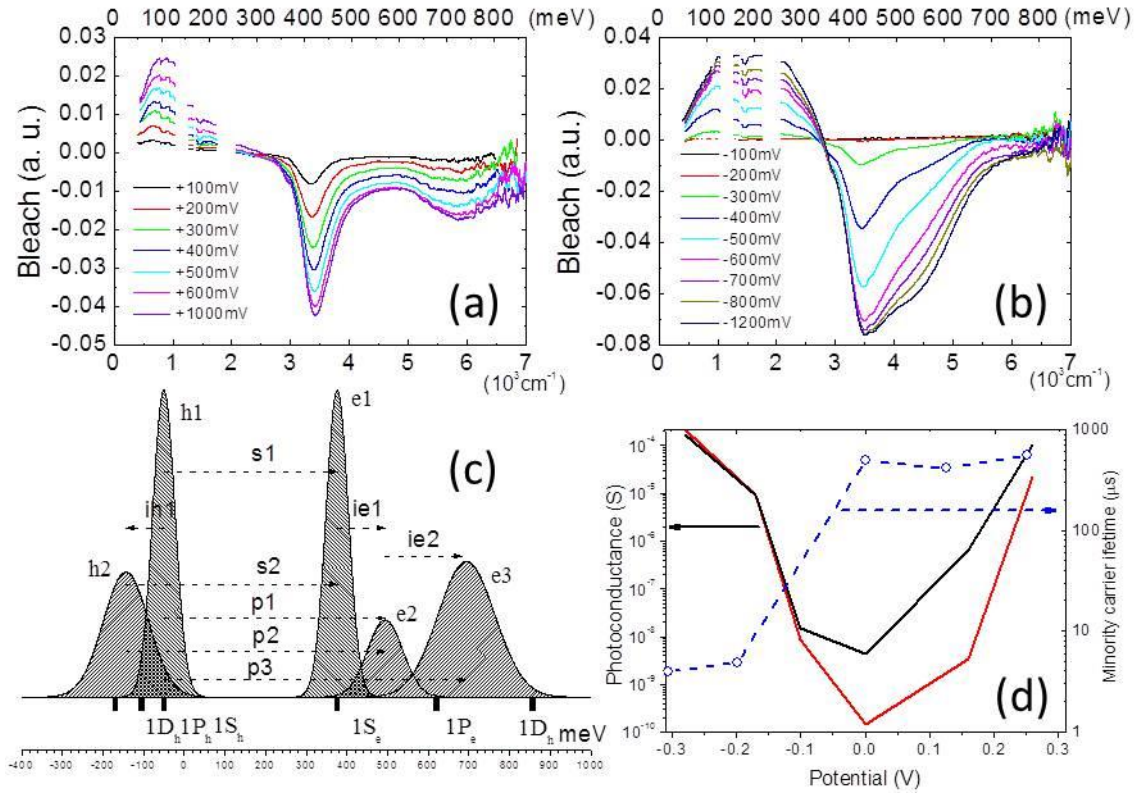


Figure 6 : (a) Bleach spectrum of a HgTe CQD film at different positive bias of the hole injection. (b) Bleach spectrum of a HgTe CQD film at different negative bias of the electron injection. (c) Reconstructed energy level diagram of HgTe CQDs with an excitonic feature around 3 µm. (d) photo (black) and dark (red) conductance of a 3µm HgTe CQD film under illumination and under dark condition as a function of the electrochemistry potential. also shown is the photocurrent decay time (minority carrier lifetime) following a short pulse from a 800nm diode laser.

A difference between transport in the narrow gap CQDs films and earlier studies on the wider gap nanocrystals of CdSe, or near-IR gap PbSe is the significant thermal carrier density. Even in an undoped or uncharged film of CQDs, i.e. intrinsic, there is a thermal carrier density which gives rise to a dark current. For the intrinsic case, the carrier density is given by:

$$n = p = N_0 \sqrt{N_c \cdot N_v} \exp(-E_G / 2k_B T) \quad (3)$$

Where $N_o$ is the density of dots per volume, $E_G$ is the dot band gap, and $N_c$, $N_v$ are the effective conduction and valence density of states per dot. For an HgTe dot with strong confinement ($E_G >> k_B T$), this was estimated as $N_c = N_v = 2$. [86] Eq. 3 then leads to one carrier per thousand nanoparticles for a 5µm cut-off CQD film at room temperature. For comparison there would be, at room temperature, only ~$10^{-17}$ thermally activated carrier per dot in a CdSe QD with a visible band edge.

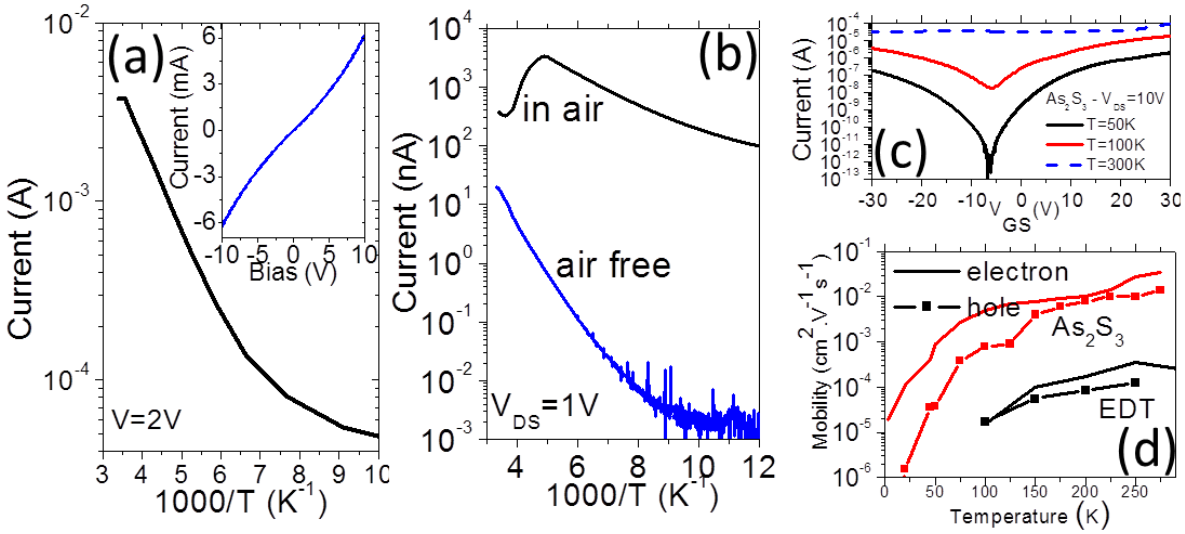


Figure 7 : (a) Current as a function of the inverse of the temperature for a film of aggregated HgTe quantum dots[86] under 2V. Inset current as a function of the applied bias at 210K. (b) Current as a function of the inverse of the temperature for a film of dispersed HgTe quantum dots ( λ≈3µm), processed with ethanedithiol in air and in a glovebox. (c) Current as a function of the gate bias for a film of dispersed HgTe quantum dots ( λ≈3µm), processed air free with $As_2S_3$. (d) Mobility as a function of the temperature for films of HgTe CQDs processed air-free with ethanedithiol or $As_2S_3$.

Transport in films of the aggregated HgTe CQDs that first allowed mid-IR photodetection was observed to be quasi-ohmic with I-V curves that are linear at room temperature and become less linear at low temperature. While such materials could have been naturally doped, it was instead found that between about 150 K and room temperature, the temperature dependence was Arrhenius with an activation energy close to half the optical band gap, as shown in Fig. 7a. [86] Following Eq. 3, these materials were therefore assigned to being intrinsic with a carrier concentration determined by the thermal excitation over the gap. From the current and the estimated carrier concentration, the carrier mobility was estimated in the $10^{-2}$ -

$10^{-1}$ $cm^2V^{-1}s^{-1}$ range. Using the Einstein relation, the inter nanoparticle hopping time was evaluated as $\tau_{hop} \approx \frac{2eR_{QD}^{\ 2}}{3\mu k_B T} \approx 13ps$ with $R_{QD}$ the CQD radius and μ is the mobility. It was then proposed that the good photodetection properties likely arose from a hopping time faster than the nonradiative recombination times.

As the synthesis improved to allow for monodisperse HgTe CQDs with better spectral properties, it was found that simply dried films were very resistive and showed no photoconduction. This was a side-effect of the better passivation due to the insulating alkane ligands. An organic ligand exchange was performed directly on such films, by dipping in a solution of short ligands dissolved in a solvent such as ethanol, which will not redissolve the film. Exchange with several thiol ligands (ethanedithiol = EDT, hexanedithiol, butanethiol, butanedithiol), and amine ligands (propylamine, butylamine, heptanediamine) was tested, giving qualitatively similar results with measureable mobility and detectivity.[87] However, the mobility of these films was in the $10^{-4}$ $cm^2$ $V^{-1}$ $s^{-1}$ range, two to three decades lower than those obtained with the aggregated material. It was also found that these films were not intrinsic, showing instead current *vs* temperature, I(T), curves with a prominent maximum, around 200K, as shown in Fig. 7b. Such rise of the conductance with decreasing temperature was attributed to temperature dependent doping and not to improved mobility at lower temperature. The conductivity was determined to be p-type by FET measurements[87] as for prior work,[81 82 83] while the increase of the carrier concentration with decreasing temperature was attributed to the temperature dependent ionization of a surface-related hole donor. The qualitative argument proposed was that the energy shift of a surface state with temperature is different from that of the HgTe band and that the conductance peak occurs when the levels cross. However, the detailed mechanism of the nonmonotonic I(T) curve has not been worked out. It was then reported that this behavior arises from air-exposure of the films during the ligand exchange, and this was attributed to the likely oxidation of the HgTe surface. Once processed under nitrogen during the ligand exchange and kept air-free, the I(T) curve of the HgTe CQDs films indicated intrinsic behavior and FET measurements showed both n and p–type mobilities.

For infrared applications of CQDs, the vibrational absorption of typical organic ligands is an impediment to high efficiencies. Ultimately, the CQDs should therefore be embedded in an IR transparent matrix, with ideally very low frequency phonons or vibrations. Different strategies have been reported for the preparation of inorganic matrices for CQD films. In one

method, CQDs films with the usual ligands coverage are subjected to a ligand exchange/removal and exposed to a few cycles of Atomic Layer Deposition (ALD).[88,89] The ALD inorganic matrix leads to improved mobility and protection of the CQDs film. However, the removal of the ligands in the films is typically not complete. As pioneered by Talapin and coworkers, it is much more effective to perform an exchange with charged inorganic ligands directly in solution.[90] A following annealing step may then be used to convert the inorganic ligands, such as hydrazinium metal chalcogenide complexes or chalcogenide ions[91] to an inorganic semiconducting matrix. This method allows for the complete removal of the organic ligands and a great flexibility in the choice of the final matrix material. In addition, vast improvements in the electronic mobility have been reported.[92] Recently, Kovalenko *et al*[93] demonstrated the use of $As_2S_3$ sol-gel for making near-IR luminescent films containing PbSe/CdS CQDs. In a related method[87] a dilute $As_2S_3$ ligand exchange solution was used to replace the organic ligands of HgTe CQD films, and to fill the interparticle spaces. $As_2S_3$ was first dissolved in propylamine and diluted in ethanol. Then films of HgTe CQD were dipped for one minute into the $As_2S_3$ solution and rinsed with ethanol. This was a simpler procedure than the liquid phase transfer of the colloidal dots but it only allowed for about a 90% removal of the organic ligands as judged by the remaining infrared CH stretching vibrations. As with the thiol ligand exchange, the ligand exchange with $As_2S_3$ must be performed in an inert atmosphere to prevent oxidation and p-type doping of the HgTe/$As_2S_3$ CQD films. With these precautions, the HgTe/$As_2S_3$ system, showed Arrhenius I(T) curves with an activation energy consistent with intrinsic behavior. As shown in Fig. 7c, n- and p-type FET were both possible with on/off ratio as high as $10^6$ at low temperature. As shown in Fig. 7d, the mobility was also improved by two orders of magnitude at room temperature compared to the ligand exchange with ethanedithiol. The improved mobility may arise from several factors, including reduced barrier height, shorter dot separation, as well as lowered charging energy from the increased dielectric constant.

For infrared detection, several other properties of the material need to be determined.[1] These are the response time, the noise, the responsivity (conversion of light to electrical current), and the detectivity (normalized signal to noise ratio).

The time response is an important property that determines the potential for imaging applications. While near-IR CQDs PbS detectors have been reported to be very sensitive, their response times were also very slow,[94] a result of some very high internal gain mechanism, associated with long lived traps. Similar results were reported with near-IR PbSe and HgTe

photodetectors.[95] In contrast HgTe CQDs photodetectors have shown fast response, of the order of the transit time, and consistent with unity gain. Fig. 8a shows the flat frequency dependence of the photocurrent in the 10Hz to 100kHz range. This is therefore promising for fast imaging applications.

Noise is a key parameter of a photodetector. Most reports on CQD-based photodetectors measure the noise only at a given frequency[84 94] but 1/f noise is important in the HgTe CQDs photodetectors, as shown in Fig. 8b. The magnitude of the *1/f* noise depends on temperature and its origin is not yet understood. Using the empirical Hooge equation, the *1/f* noise magnitude is characterized by the $\alpha_H$ parameter with $i_{1/f}{}^2 = \frac{\alpha_H \cdot I^2}{N \cdot f}$, where *f* is the signal frequency, *I* the current, *N* the total number of carriers involved in transport and $i_{1/f}$ is the noise current density. Values for bulk crystalline materials are $10^{-6}$-$10^{-3}$. However, a value of $\alpha_H$ ~ 0.4 was reported for a HgTe CQD film[86] based on estimates of carrier density and this is in large excess compared to single crystal materials. Future studies of film processing should shed light on the origin of the large excess noise in the CQD films and possibly lead to lowering the 1/f noise. This will then allow for improved detectivity.

The responsivity of a photoconductor is the ratio of photocurrent to incident optical power, in A.W$^{-1}$ (or V$^{-1}$). It can be expressed as $R = \frac{G\eta}{E_g}$ where *G* is the gain, $\eta$ is the external quantum efficiency, and $E_g$ is the gap energy in Volts. With a unity gain and 100% quantum yield, the responsivity of a 2 micron detector would be 1.5 A.W$^{-1}$. HgTe CQDs processed with $As_2S_3$ have very fast response time, of the order of the expected transit time suggesting that there is no significant gain. Such a detector at 2 microns showed a responsivity of 0.65 A.W$^{-1}$, as shown in Fig.8c, which is consistent with an external quantum efficiency of 50%. For longer wavelength detection with HgTe CQDs in the mid-IR, at 3.5 microns, the responsivity is lower, around 0.22 A.W$^{-1}$ indicating that an order of magnitude improvement is still possible in the quantum efficiency. *A priori*, improvement of the responsivity will arise from an understanding of the nonradiative recombination processes and progress in the surface control of the CQDs.

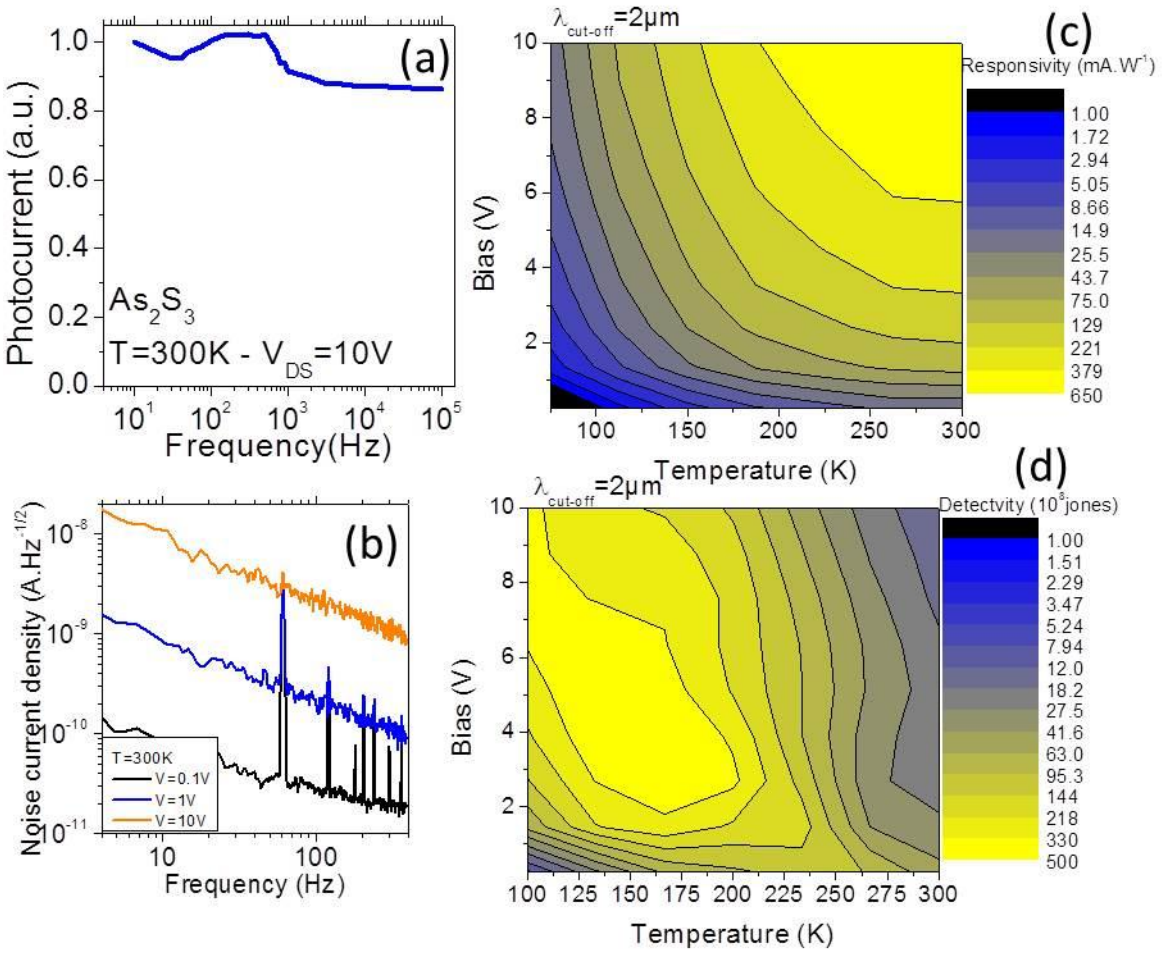


Figure 8: (a) Photocurrent as a function of the frequency of the light modulation for an illumination by a 800nm laser (b) Noise current spectral density at room temperature and under different bias. (c) and (d) are respectively the map of the responsivity and detectivity as a function of the bias and temperature for a film of HgTe CQD film with a cut-off wavelength at 2µm

The detectivity of a photoconductor is the inverse of the power equivalent to the noise, normalized per area and bandwidth. It is obtained as $D^* = \frac{R\sqrt{A}}{i_n}$ where $R$ is the responsivity, $A$ is the detector area, and $i_n$ is the current noise spectral density ($A/Hz^{1/2}$) at the chosen frequency. The unit of D* is Jones=$cmHz^{1/2}W^{-1}$. If the noise depends on frequency, D* must then specify the frequency at which it is measured. For thermal imaging, the minimum current noise arises from the background thermal radiation noise, typically at 300K. In addition, there is the Johnson noise, shot noise, recombination-generation noise due to the thermal excitation

of the carriers, and 1/f noise. The standard DTGS detectors used in commercial FTIR have a detectivity of ~ 2x $10^8$ at a 1 kHz frequency, but they operate without cooling and cover the whole IR range. The liquid Nitrogen cooled MCT detectors in commercial FTIR with response up to 12 microns have a detectivity of ~ 6 x $10^{10}$ Jones. With near-IR PbSe CQDs, a detectivity of $10^{13}$ Jones has been reported, although with a slow response of tens of Hz. In general, the maximum D* decreases rapidly with longer wavelength due to the increased thermal background. For a 3.5 μm cut-off HgTe/$As_2S_3$ at 200 K, with faster than 100kHz response, a detectivity of $3.5\times10^{10}$ Jones at 1kHz was obtained.[8787] This was not an optimized value as the films remained too thin to fully absorb the IR radiation and further improvements are expected. To put this result into context, a photoconductor at 3.5 microns limited by the 2π 300K thermal radiation would have an ideal detectivity of $8x10^{11}$ Jones and this is nearly reached with commercial cooled InAs detectors. Therefore there is a factor of about 20 to gain with further material development of the HgTe CQDs.

**V. Conclusion and Perspective**

As soluble materials with a priori well defined infrared electronic properties, CQDs potentially cover a high cost technological area that is inaccessible to organics. The earlier studies of CQDs with the mid-IR intraband (e.g. CdSe) and the near-IR interband transitions (e.g. PbSe) gave a preview of their potential in the infrared. At present, the most promising material is HgTe. The inverted band structure of HgTe has long generated interest, in particular for the use of HgCdTe alloy for infrared detection and more recently with the demonstration of the surface protected states and topological insulators. Over the past decade and a half, the colloidal synthesis of HgTe CQDs has steadily evolved, allowing for larger and larger dots and improved monodispersivity. HgTe CQDs of 12-14 nm are currently the largest synthesized, and their room temperature band edge absorption and luminescence reaches 5 μm.

Photodetectors made with HgTe CQDs films have been demonstrated across the mid-IR, and up to 7 μm due to the red shift of the band edge upon cooling. The close-packed HgTe CQDs films present a large absorption ($\alpha>10^4 cm^{-1}$) compatible with thin film devices. Anhydrous electrochemistry has shown that the HgTe CQDs are stable under both n- and p- type charging. Ambipolar mobility of the HgTe CQDs films has also been observed with solid state FETs. The transport properties of films of HgTe CQDs have been improved by exchanging the organic ligands for an inorganic $As_2S_3$ matrix. At present, there is a little more than one order of magnitude to gain with the HgTe CQDs to bring the single detector

performance on par with the best epitaxial materials in the MWIR. The good performances have to be extended to LWIR and this requires progress in the synthesis of larger CQDs. Improved responsivities are likely to arise from understanding and eliminating the nonradiative processes, possibly with the introduction of core/shell systems such as the lattice matched HgTe/CdTe. This would also allow for new applications of the CQDs as mid-IR emitters. They might then be good materials for down converting existing visible LEDs or near-IR laser diodes to make mid-IR light sources and lasers. In parallel the development of inorganic matrix materials with infrared transparency, the complete elimination of organics, and somewhat higher mobility will lead to improved optoelectronic properties, and it is likely that HgTe/$As_2S_3$ is not yet the optimum material. There is also a need for understanding the source of the excess electrical noise in these granular nanomaterials, since the understanding may lead to less noisy material and improved detectivity at low frequencies, an important problem for the pixel calibration of infrared cameras. The *a priori* versatile processing of the colloidal materials will allow an easy integration with plasmonic antenna structures which should further decrease the noise by reducing the volume of the active material, or allow higher operating temperatures. The rapid progress over the past couple years suggests that such improvements may be within reach. At present, the HgTe CQDs appear as a very attractive alternative technology for infrared detection and imaging, justifying further basic studies of their optical properties, further material development, and integration into devices.

**Acknowledgements:** The work on HgTe CQDs is funded by the DARPA COMPASS program with a grant from ARO. The infrared photophysics research program is funded by the National Science Foundation DMR-1104755, and studies of electrical transport are funded by the US Department of Energy (DOE) under Grant No. DE-FG02-06ER46326.

## VI - References


[1] Rogalski, A., *Infrared Phys. and Tech*. **2011**, 54, 136

[2] Schneider H.; Liu H. C., in Quantum well infrared photodetectors: physics and applications Springer, Berlin (2006)

[3] Levine B.F. *J. Appl. Phys***. 1993**, 74, R1

[4] Sundaram, M .; Reisinger, A.; Dennis, R.; Patnaude, K.; Burrows, D.; Bundas, J.; Beech, K.; Faska, R., *Infrared Phys. and Tech*. **2011**, 54, 194

[5] Mailhiot, C; Smith, DL, *J. Vac. Sci. & Tech.* **1989,** A7, 445

[6] Chow D. H.; Miles R.H.; Schulman J.N.; Collins D.A.; McGill T.C. *Semicond. Sci. Techno*. **1991**, 6, C47

[7] Y. Wei, M. Razeghi, *Phys. Rev. B*, **2004**, 69, 085316.

[8] Ekimov A. I. , Onushchenko A. A. *JETP Lett*. **1981**, 34, 345

[9] Efros Al.L.; Efros A.L. *Soviet Phys. Semiconductors* **1982**, 16, 772

[10] Brus L.E. J. *Chem. Phys*. **1983**, 79, 5566.

[11] Murray C. B.; Norris D. J.,. Bawendi M. G., *J. Am. Chem. Soc*.**1993**, 115, 8706.

[12] Talapin, D., Lee, J., Kovalenko, M. & Shevchenko, E. *Chem. Rev.* **110**, 389 (2010).

[13] Klimov, V. I. *Nanocrystal Quantum Dots, Second Edition*. (Taylor and Francis: Boca Raton, Fl, 2009).

[14] Hines M.A. ; Guyot-Sionnest P., *J. Phys. Chem*. **1996**, 100, 468.

[15] Reiss P., Protiere,M., Li, L, *Small*, **2009**, 5, 154.

[16] Igor L.; Medintz H.; Uyeda T.; Goldman E.R.; Mattoussi H. *Nat. Mat*. **2005**, 4, 435.

[17] See the article by Bulovic and Bawendi in this special edition of *Chem.Mat*.

[18] Wise, F.W., *Acc. Chem. Res*. **2000**, 33, 773

[19] Murray, C. B.; Sun, S. H.; Gaschler, W.; et al. *IBM. J. Res. De*v. **2001**, *45*, 47.

[20] Wehrenberg B.L.; Wang C.; Guyot-Sionnest P. *J. Phys. Chem. B* **2002**, 106, 10634

[21] Du, H.; Chen, CL.; Krishnan, R.; Krauss, T.D.; Harbold, J.M.; Wise, F.W.; Thomas, M.G.; Silcox, J. *Nano Lett.* **2002**, 2, 1321

[22] Koleilat G.I.; Levina L., Shukla H.; Myrskog S.H.; Hinds S.; Pattantyus-Abraham A.G.; Sargent E H., *Nano Lett*. **2008**, 2, 833.

[23] Rauch T.;Böberl M.; Tedde S.F.; Fürst J.; Kovalenko M.V.; Hesser G.; Lemmer U.; Heiss W.; Hayden O. *Nature Nano* **2009**, 2, 332.

[24] Tang J.; Sargent E. H. *Advanced Materials* **2011**, 23, 12.

[25] Luther J.M.; Gao J.; Lloyd M.T.;Semonin O.E.;Beard M.C.;Nozik A.J.; *Adv. Mat*. **2010,** 22, 3704.

[26] Semonin, O. E.; Luther, J. M.; Choi, S.; Chen, H. Y.; Gao, J. B.; Nozik, A. J.; Beard, M. C. *Science* **2011**, 334, 1530−1533.

[27] Guyot-Sionnest P. ;Hines M.A. *Appl. Phys. Lett*. **1998**, 72, 686.

[28] Shim M, Guyot-Sionnest P Nature **2000**, 407 981

[29] Wang C.J., Shim M., Guyot-Sionnest P. *Science* **2001**, 291 2390.

[30] Blackburn J.L., Ellingson R.J.,Micic, O.I., Nozik A.J., *J. Phys. Chem. B* **2003**, 107, 102

[31]Wang C.J.; Shim M. ; Guyot-Sionnest P. *Appl. Phys. Lett*. **2002**, 80, 4

[32] Erwin S.C. ; Zu l. ; Haftel M.I. ; Efros A. L. , Kennedy T.A. ; Norris D.J. ; *Nature* **2005**, 436, 91.

[33] Buonsanti R, Llordes A, Aloni S, Helms BA, Milliron DJ, *Nano Lett*. **2011**, 11, 4706

[34] Luther, JM , Jain, PK, Ewers, T, Alivisatos, A.P., *Nature Mat*. **2011**, 10, 361

[35]Shim M, Shilov SV, Braiman MS, Guyot-Sionnest P. *J. Phys. Chem B* **2000**, 104, 1494

[36] Pietryga, J.; M. Schaller, R. D.; Werder, D.; Stewart, M. H.; Klimov, V. I.; Hollingsworth, J. A. *J. Am. Chem. Soc.* **2004**, *126*, 11752.

[37] Guzelian A.A.; Banin U.; Kadavanich A.V.;Peng X.; Alivisatos A. P. *Appl. Phys. Lett***. 1996**, 69, 1432.

[38] Harris D. K.; Allen P. M.; Han H. S.; Walker B.J.; Lee J.: Bawendi M. G. *J. Am. Chem. Soc*. **2011**, 133, 476

[39] Ayaskanta S.; Lejun Q.; Moon Sung K.; Deng D.; Norris D.J. *J. Am. Chem. Soc.* **2011**, 133, 6509.

[40] Sahu A.; Khare A.; Deng D.D.; Norris D.J. *Chem. Commun* **2012**, 48, 5458.

[41] Arachchige I.U., Kanatzidis M.G., *Nano lett*. **2009**, 9, 1583.

[42] Ryzhii V., Maxim Ryzhii M., Ryabova N., Mitin V., and Otsuji T., Jpn. J. Appl. Phys. 2009, **48**, 04C144

[43] Stankiewicz J.; Giriat W. ; Bienenstock A. *Phys. Rev. B* **1971**, 4, 4465.

[44] Szlenk K. *Phys Stat. Sol. (b)* **1979**, 95, 445.

[45] Z. Dziuba, *Phys Stat. Sol. (b)* **1983**, 118, 319.

[46] Bastard G.; Guldner Y.; Rigaux C.; N'guyen H.H.; Vieren J.P.; Menant M.; Mycielski A. *Physics Letters A* **1973**, 46, 99.

[47] Liu L. ; Verié C. *Phys. Rev. Lett.* **1976**, 37, 453.

[48] Groves S. H. ; Brown R. N. ; Pidgeon C. R., *Phys. Rev*. **1967**, 161, 779 .

[49] Nimtz G.; Schlicht B in Narrow gap semiconductors, Spinger tracts in modern Physics, vol 98, Berlin **1983**

[50] Man P.; Pan D S. *Phys. Rev. B* **1991**, 44, 8745.

[51] Baars J.; Sorger F. *Sol.State Comm*. **1972**, 10, 875

[52] Kepa H.; Giebultowicz T.; Buras B.; Lebech B.; Clausen K. *Phys. Scr*. **1982,** 25, 807.

[53] Hasan M.Z.; Kane C.L., *Rev. Modern. Phys*. **2010**, 82, 3045.

[54] König M.; Wiedmann S.; Brüne C.; RothA.; Buhmann H.; Molenkamp L.W.;. Qi X. L.; Zhang S.C., *Science* **2007**, 318, 766.

[55] Rogach A, Kershaw S, Burt M., Harrison M, Kornowski A, Eychmüller A, Weller H, *Adv. Mater*. **1999**, 11, 552.

[56] Harrison M.T.; Kershaw S.V.; Burt M.G.; Rogach A.; Eychmüller A.; Weller H. *J. Mat. Chem*. **1999**, 9 2721.

[57] Harrison M.T.; Kershaw S.V.; Burt M.G.; Eychmuller A.; Weller H.; Rogach A.L., *Mater. Sci. Eng. B* **2000**, 335, 69.

[58] Kovalenko M. V., Kaufmann E., Pachinger D., Roither J., Huber M., Stangl J., Hesser G., Schäffler F., Heiss W., J. *Am. Chem. Soc*. **2006**, 128, 3516.

[59] Tang B.; Yang F.; Lin Y.; Zhuo L.; Ge J.; Cao L. *Chem. Mater*. **2007**, 19, 1212.

[60] Kershaw S.V. ; Burt M. ;Harrison M. ; Rogach A. ;Weller H. ; Eychmüller A. *Appl. Phys. Lett*. **1999**, 75, 1694

[61] Smith A.M.; Nie S. *J. Am. Chem. Soc.* **2011**, 133, 24

[62] Lesnyak V.; Lutich A.; Gaponik N.; Grabolle M.; Plotnikov A.; Resch-Genger U.; Eychmüller A. *J. Mat. Chem*. **2009**, 19, 9147.

[63] Sun H.; Zhang H.; Ju J.; Zhang J.; Qian G.; Wang C.; Yang B.; Wang Z.Y. *Chem. Mater*. **2008**, 20, 6764.

[64] Green M., Wakefield G.a Dobson P.J. *J. Mater. Chem.*, **2003**, 13, 1076–1078

[65] Piepenbrock M.O.M.; Stirner T.; Kelly S.M.; O'Neill M. *J. Am. Chem. Soc*. **2006**, 128, 7087.

[66] Keuleyan S.; Lhuillier E.; Brajuskovic V.;Guyot-Sionnest P. *Nat Photon* **2011**, 5, 489

[67] Keuleyan S.; Lhuillier E.; Guyot-Sionnest P. *J. Am. Chem. Soc.* **2011**, *133*, 16422.

[68] Lhuillier E.; Keuleyan S.; Guyot-Sionnest P. *Nanotechnology* **2012**, 23, 175705.

[69] Olkhovets A.; Hsu R.-C.; Lipovskii A.; Wise F W *Phys. Rev. Lett*. **1998**, 81, 3539.

[70] Valerini D.; Cretí A.; Lomascolo M.; Manna L.; Cingolani R.; Anni M. *Phys. Rev. B* **2005**, 71, 235409.

[71] Dai Q,Yu Z., Zhang Y,Wang Y, Hu M.Z., Zou B.,Wang Y, Yu W.W. *Langmuir* **2010**, 26**,** 11435

[72] Nimtz G.; Schlicht B. in Narrow gap semiconductors, Spinger tracts in modern Physics, vol 98, Berlin 1983.

[73] Blue M D. *Phys. Rev*. **1964**, 134, A226.

[74] Norton P *Opto-Electronics Rev*. **2002**, 10, 159.

[75] Rogalski A. *Rep. Prog. Phys*. **2005**, 68, 2267.

[76] Semonin, O.E.; Johnson, J.C.; Luther, J.M.; Midgett, A.G.; Nozik A.J.; Beard, M.C., J. Phys. Chem. Lett. **2010**, 1, 2445

[77] Liu H.; Guyot-Sionnest P., *J. Phys. Chem*. C **2010**, 114, 14860.

[78] Guyot-Sionnest P. ; Wehrenberg B.;, Yu D. *J. Chem. Phys*. 2005, 123074709.

[79] Aharoni, A.; Oron, D.; Banin U.; Rabani, E.; Jortner, J. *Phys. Rev. Lett*. **2008** 100, 057404

[80] Pandey A, Guyot-Sionnest P *Science* **2008,** 322, 929

[81] Kim H.; Cho K.; Kim D.W.; Lee H.R. Kim S. *Appl. Phys. Lett*. **2006**, 89, 173107.

[82] Yun J.; Cho K.; Kim S. *Nanotechnology* **2010**, 21, 235204.

[83] Kim D.; Jang J.; Kim H.; Cho K.; Kim S. *Thin Solid Films* **2008**, 516, 7715.

[84] Böberl, M., Kovalenko M.V., Gamerith, S., List E.J.W., and Heiss W., *Adv. Mater.* **2007**, *19*, 3574.

[85] Allan G, and Delerue C. *Phys. Rev. B* **2012**, 86, 165437.

[86] Lhuillier E. ; Keuleyan S.; Rekemeyer P. ; Guyot-Sionnest P. ;J. *Appl. Phys* **2011**, 110, 032110.

[87] Lhuillier E ; Keuleyan S. ; Zolotavin P. ;Guyot Sionnest P , *Adv Mat* **2013**, 25, 137.

[88] Ihly R.; Tolentino J.; Liu Y.; Gibbs M.; Law M. *ACS Nano* **2011**, 5, 8175.

[89] Pourret A.; Guyot-Sionnest P.; Elam J.W. *Adv. Mat*. **2008**, 20, 1.

[90] Kovalenko M.V.; Scheele M.; Talapin D.V. *Science* **2009**, 324, 1417.

[91] A. Nag, M. V. Kovalenko, J. S. Lee, W. Y. Liu, B. Spokoyny, and D. V. Talapin, *J. Am. Chem. Soc.* **2011,** 133, 10612

[92] Lee J.S., Kovalenko M.V., Huang J., Chung D.S. and Talapin D.V., *Nature Nanotech* **2011**, 6, 348.

[93] Kovalenko M.V.; Schaller R. D.; Jarzab D.; Loi M. A.; Talapin D.V., *J. Am. Chem. Soc*. **2012**, 134, 2457

[94] Konstantatos G., Howard I., Fischer A., Hoogland S., Clifford J., Klem E., Levina L. ; Sargent E.H., *Nature* **2006**, 442, 180

[95] Böberl M., Kovalenko M.V. , Gamerith S., List E.J. W., and Heiss W. , *Adv. Mater*. **2007**, 19, 3574–3578